Hindawi
Mathematical Problems in Engineering
Volume 2020, Article ID 1067215, 14 pages
https://doi.org/10.1155/2020/1067215

Research Article

Engineering Application and Prediction of the Influence Area of the Rockfall Hazards

Xiaohui Liao,[1] **Xueliang Wang**,[2,3,4] **Lihui Li**,[2,3,4] **Haiyang Liu**,[2,3,4] **Zhifa Yang**,[2,3,4] **and Zigan Chen**[5]

[1]*College of Civil Engineering and Architecture, Quzhou University, Quzhou 324000, China*
[2]*Key Laboratory of Shale Gas and Geoengineering, Institute of Geology and Geophysics, Chinese Academy of Sciences, Beijing 100029, China*
[3]*College of Earth and Planetary Sciences, University of Chinese Academy of Sciences, Beijing 100049, China*
[4]*Innovation Academy for Earth Science, Chinese Academy of Sciences, Beijing 100029, China*
[5]*Zhejiang Shenxianju Tourism Group Co., Ltd., Taizhou 317300, China*

Correspondence should be addressed to Xiaohui Liao; liaoxiaohui@sina.com

Received 24 December 2019; Revised 20 March 2020; Accepted 8 April 2020; Published 7 May 2020

Academic Editor: Benjamin Ivorra

The identification of potential rockfall and the accurate prediction of its trajectory are critical in prevention and mitigation of rockfall hazard. It is an important precondition to assess the uncertainty of rockfall motion, study the effective identification technology of potential rockfall, predict the rockfall trajectory, and calculate the threatened area by rockfall hazards. In this study, field investigations and numerical simulations were carried out to identify potential rockfall on a weathered rock slope. As a case study, our calculations results show that the area of tensile stress concentration and plastic failure is the potential area where the rockmass will fall off the surface of the weathered rock slope. A mathematical model for calculating the rockfall influence area of the weathered rock slope was established based on the optimization theory, neural network technology, and genetic optimization algorithm. The rockfall influence area of the weathered rock slope was determined using maximum horizontal distance of rockfall in the specified slope cross sections and described on the topographic map using spline curves to form a closed possibly vulnerable area. As a case study, our calculations confirm that the distributions of the plastic failure and tensile stress areas obtained from the numerical simulations are consistent with the dangerous rock masses identified by field investigations at Guanyindong Slope that is a popular tourist scenic spot in Zhejiang Province, China. In this study, it has been indicated that the influence area can be used as the basis for the design of passive protection methods for rock slopes vulnerable to rockfall hazards.

1. Introduction

Rockfall is a common geological disaster that occurs during any construction activities in the mountainous region. Because rockfalls are random and destructive, the trajectory of rockfalls has not been effectively predicted. These disasters can result in enormous losses to any construction projects and tourism sites in the hilly/mountainous areas.

In recent years, many studies have been conducted on the controlling factors and motion characteristics of rockfalls using theoretical analysis [1], field investigations [2–4], statistical analysis [5], field tests [6–8], and numerical simulation analysis [9]. Previous models can be divided into three groups: empirical models [3, 10–12], analysis and calculation models based on the theory of kinematics [5, 10, 13–19], and mathematical models based on Geographic Information System (GIS) [20–22]. Empirical models usually require a great deal of field investigation and experiments for statistical analysis and thus consume a great amount of manpower and financial resources. Formulas based on empirical models are often only locally applicable. Both analysis and calculation models based on the theory of kinematics and mathematical models based on GIS require a large number of input parameters related to slope morphology and rolling blocks' characteristics, which are usually not readily available.

All of the above-mentioned studies satisfactorily explain the characteristics of the rockfall motion of the slope and provide a theoretical basis for the prevention and control of rockfall hazards. However, it is impossible to use empirical formulas or specific mathematical expression to accurately predict the potential trajectory of dangerous rockmasses after falling because the trajectory is closely related to the complex and variable slope parameters (e.g., the shape of the slope, the slope's vegetation cover, and the shape and size of the blocks). Due to many factors controlling rockfall, the slope roughness exerts a limiting effect on the lateral motion of the rockfall, especially for steep rock slopes [15, 23]. In addition, several complex parameters are required to simulate the three-dimensional rockfall run-out, which increases the level of uncertainty. However, it is feasible to approximate the rockfall motion as a planar motion for a steep rock slope with a relatively smooth surface [24]. Taking the Guanyindong Rock Slope, which is located in a tourist scenic spot in Zhejiang Province, China, as an example, field investigations and numerical simulation analysis were used to identify potential dangerous rockmass. In addition, the neural network technique was used to calculate the influence area of rockfall. Based on field investigation and numerical simulation results, a corresponding mathematical model for determining the influence range was established, and the maximum run-out distance of the potential rockfall was computed using a genetic optimization algorithm. This study provides a basis for the design of passive preventative methods for preventing rockfall.

2. Calculation Theory of the Influence Area of Rockfall

Authors have established the model to calculate the run-out distance of rockfall. This model can calculate the maximum run-out distance of rockfall at a specific profile of the rock slope.

2.1. Basic Assumptions. For any profile of a steep slope that weathers easily, the slope's shape, slope angle, the accumulation at the toe of the slope, and the amount of vegetation covering on the slope's surface are all fixed constants. Historical rockfall data also shows that the mass of the rockfall block and its location usually change. Therefore, in this study, the following assumptions are made to establish a model for calculating the horizontal distance of the rockfall for any slope profile.

(1) The rockfall motion is a planar motion.

(2) The initial velocity of the dangerous rock mass at the start of the rockfall is zero.

(3) For any given profile of the slope, the mass of the dangerous rock mass and the position of the rockfall block are variables.

2.2. Establishment of the Local Coordinate System. Based on the above assumptions, a local coordinate system was established for the slope (see Figure 1). The x axis was defined as the direction of the slope's surface; the z axis was defined as the elevation direction of the slope; and the y axis was defined as the direction perpendicular to the paper.

2.3. Basic Equations and Analysis. It is assumed that rockfall occurs for any section $x = x_i$ and that rockfall has a planar motion. Also, it is assumed that, at the beginning of the rockfall motion, the position of the dangerous rockmass v is (x_i, y_i, z_i), the mass of the potential rockfall is m_v (kg), and the position after the rockfall of the dangerous rockmass is (x_j, y_j, z_j). For section $x = x_i$, the dangerous rockmass v rockfall and the resulting horizontal distance of the motion are

$$D_{v,\,x=x_i} = y_j - y_i = f(z, m_v),\ v = 1, 2, 3, \ldots, n_1;\quad i = 1, 2, 3, \ldots, n_2. \tag{1}$$

If $f_{x_i}(z, m_v) = f(z, m_v) + y_i$, then

$$y_j = f_{x_i}(z, m_v). \tag{2}$$

In the above formulas, $D_{v,x=x_i}$ is the rockfall horizontal distance (m) of the dangerous rockmass v at cross section $x = x_i$ of the slope, and f and f_x are the rockfall motion functions.

The calculation of the maximum horizontal distance of the rockfall at cross profile $x = x_i$ can be converted into an optimization problem expressed as follows:

$$\begin{aligned} &\max \quad y_{x=x_i} = \max f_{x_i}(z, m_v), \\ &\text{s.t} \quad \begin{cases} x_i \geq 0, \\ z \geq 0, \\ m_v \geq 0, \end{cases} \end{aligned} \tag{3}$$

where v is the number of the dangerous rockmasses at profile $x = x_i$; i.e., $v = 1, 2, 3, \ldots, n_1$; and i is the number of the cross sections of the slope; i.e., $i = 1, 2, 3, \ldots, n_2$.

To solve the optimality theory problem expressed by (3), the position of the dangerous rockmass where the weathered slope may be rockfall, i.e., the range of the x and z values, is determined first. For convenience, a finite number of profiles were defined along the x direction of the slope, the maximum rockfall horizontal distance of each profile was calculated and marked on the topographic map, and a spline curve was used to connect all of the points to form an enclosed area; this area represents the influence area of the weathered slope rockfall.

2.4. Constraints. As shown in (2) and (3), the calculation of the influence area of the rockfall at profile $x = x_i$ requires that the position z and mass m (kg) of the rockfall dangerous rock mass, i.e., the constraints of the model in (3), be determined as follows.

2.4.1. Position Constraints for the Rockfall Dangerous Rockmass. The rockfall and spalling of a rock slope are the results of the interaction of various external forces. Rockfall occurs due to a combination of the rockmass gravity and external forces, such as fissure water pressure, expansion

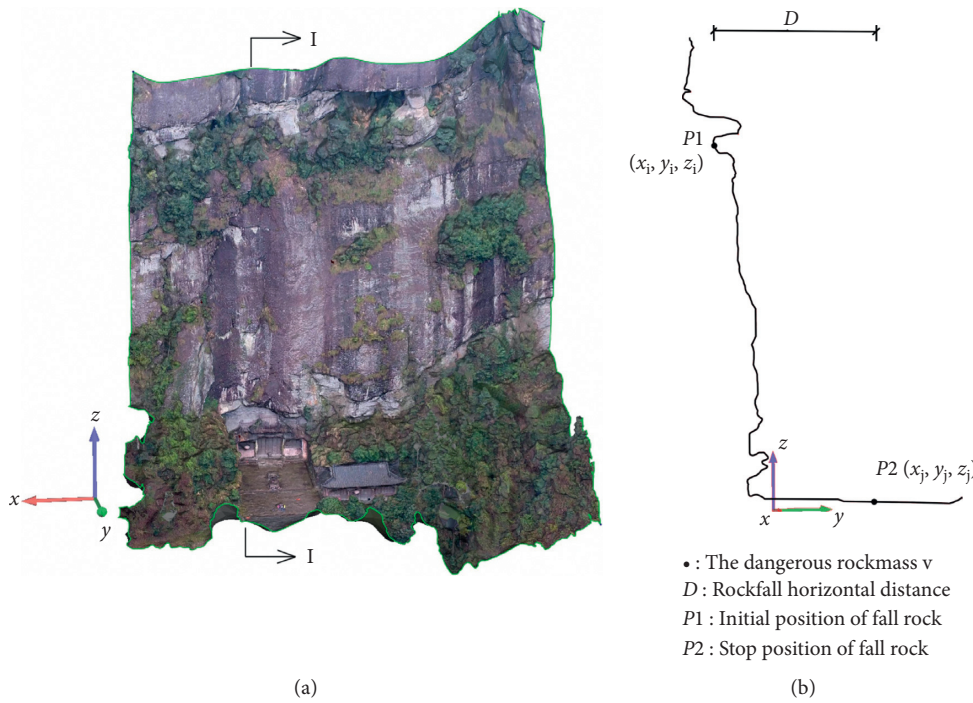

Figure 1: The coordinate system for the rockfall horizontal distance calculation model. (a) Weathered rock slope surface. (b) Cross profile I-I.

pressure exerted by plant roots, and weathering, which is caused by high-steep slopes and steeply inclined fissures. Examples of this failure include brittle tensional cracks in the surface of the rockmass under low stress conditions, spalling of the surface rockmass due to the close relationship between the rockmass structure and the stress state of the rockmass, and cantilever failure, which is the formation of tensional cracks caused by the shear failure or plastic failure of the rockmass in the rock cavity area under high stress conditions. Therefore, the tensile stress distribution and the plastic failure inside the rockmass of steep weathered slopes are important conditions that can accelerate the occurrence of rockfall. Accordingly, the area where the slope may be rockfall can be identified and used as the position constraints needed to calculate the horizontal distance of the rockfall motion.

FLAC^{3D} is a 3D numerical simulation software developed by ITASCA that is commonly used in geotechnical engineering. FLAC^{3D} uses the explicit difference scheme to solve the governing differential equation of the field. Therefore, it can satisfactorily simulate characteristics such as the internal stress state, the yield failure, and the plastic flow of the rockmass. In addition, it can be used to analyze the 3D spatial deformation behavior of a rockmass after it reaches the yield limit [25] and to determine the plastic failure zone and the tensile stress concentration of the rockmass. In order to determine the position range of the dangerous rockmass and where it may be rockfall, we used FLAC^{3D} to calculate the tensile stress zone and plastic failure zone at any position on the slope's surface. Based on this, the detailed slope failure conditions of the site can be used to determine the two zones, and the highly overlapping zone of the two can be used as the position constraints for the dangerous rockmass that may be rockfall.

2.4.2. Mass Constraints of the Collapsing Dangerous Rockmass. The rock mass with potential rockfall was determined using the following methods:

(1) A detailed investigation of historical rockfall of the steep weathered slope was conducted. The shape, size, location, and distance of the rockfall block were counted and analyzed in the detailed investigation, so as to determine the volume for the historical rockfall mass.

(2) Unmanned aerial vehicle (UAV) tilt photography modeling and 3D laser scanning techniques were employed to establish a 3D numerical model of the slope mass and to identify and measure the size of the dangerous rockmass that could be rockfall.

(3) According to the Engineering Rockmass Test Method Standards (GB/T 50266-2013) (Ministry of Housing and Urban Rural Development of People's Republic of China 2013) [26], drill core sampling (ϕ 50 mm × 100 mm in size, 5 samples in each group) is conducted in different areas depending on types of rock present on the slope, and then laboratory tests were conducted to obtain the physical and mechanical parameters of the rock samples, including the natural density of the slope mass. The masses ($m = \rho v$) of various dangerous rockmasses determined from steps 1 and 2 were calculated and ranked in ascending order; $[m_{\min}, m_{\max}]$ is the mass constraint range of the rockfall dangerous rockmass.

2.5. Model Solution

2.5.1. Calculation of the Horizontal Distance of the Rockfall. Due to the randomness of the rockfall, the function of the horizontal distance of the rockfall motion $y = f_x(z, m)$ is uncertain for any cross profile of the weathered slope; i.e., the functional mapping relationship between the horizontal distance of the rockfall y, the rockfall block position coordinate z, and the mass of the rockfall block m cannot be described by an exact expression. However, based on the uncertainty function's mapping relationship, the BP (backpack) neural network can learn the rules of the corresponding function by analyzing the sample data; thus, the result closest to the expected output value can be obtained given an input value [27, 28]. As a result, the BP neural network can be used to express the function of the horizontal distance of the rockfall $y = f_x(z, m)$; see Figure 2.

(1) Establishment of the Network Model. We propose the fact that the structural model of the BP neural network of the horizontal distance of the rockfall function has the three hidden layer neural network structure shown in Figure 2.

(2) The Input Layer. The input layer includes the position coordinate z of the dangerous rockmass and the mass m of the dangerous rockmass. The input layer can be expressed in vector form as $X = (z, m)^T = (x_1, x_2)^T$.

(3) The Hidden Layer. The output vector of each hidden layer is expressed as $U^3 = (u_1^3, u_2^3, \ldots, u_{m3}^3)^T$, $U^2 = (u_1^2, u_2^2, \ldots, u_{m2}^2)^T$, and $U^1 = (u_1^1, u_2^1, \ldots, u_{m1}^1)^T$. The weight matrix from the input layer to the hidden layer is $V^1 = (v_1^1, v_2^1, \ldots, v_{m1}^1)^T$, $V^2 = (v_1^2, v_2^2, \ldots, v_{m2}^2)^T$, and $V^3 = (v_1^3, v_2^3, \ldots, v_{m3}^3)^T$. The column vector v_j^i is the weight vector corresponding to the jth neuron of the ith hidden layer. If the threshold of the neuron is T_i, then

$$u_j^3 = f\left(\text{net}_j\right), \text{net}_j = \sum_{i=0}^{m_2}\left(v_{ij}^3 u_i^2 - T_i^2\right), j = 1, 2, \ldots, m_3, \quad (4)$$

$$u_j^2 = f\left(\text{net}_j\right), \text{net}_j = \sum_{i=0}^{m_1}\left(v_{ij}^2 u_i^1 - T_i^1\right), \ j = 1, 2, \ldots, m_2. \quad (5)$$

$$u_j^1 = f\left(\text{net}_j\right), \text{net}_j = \sum_{i=0}^{2}\left(v_{ij}^1 x_i - T_i^0\right), \ j = 1, 2, \ldots, m_1. \quad (6)$$

(4) The Output Layer. The output layer is the value of the horizontal distance of the rockfall motion, which can be expressed by the vector $O = (o_1)^T$. The rockfall horizontal distances from investigations of historical rockfalls or from numerical simulation are taken as the expected output value, which can be expressed by the vector $d = (d_1)^T$. This value can be used as the basis for the neural network, which can be used to calculate and adjust the weights of the output layer and the hidden layers. If the weight matrix between hidden layer 3 and the output layer is $d = (\omega_1)^T = (\omega_{11}, \omega_{21}, \ldots, \omega_{m_3 1})$, the output layer can be expressed as

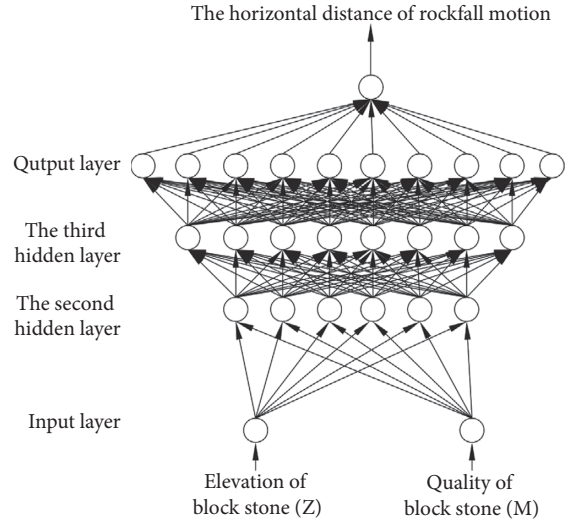

Figure 2: The rockfall horizontal distance calculation model.

$$o_1 = f\left(\text{net}_j\right),$$
$$\text{net}_j = \sum_{i=0}^{m_3}\left(\omega_{i1} u_i^3 - T_i^4\right). \quad (7)$$

(5) The Transfer Function. The unipolar Sigmoid function was used for the transfer functions of both the output layer and the hidden layer [29]:

$$f(x) = \frac{1}{1 + e^{-x}}. \quad (8)$$

In summary, when using the neural network model, as shown by (4) through (8), as the model for calculating the horizontal distance of the rockfall motion, as shown in (2), it is necessary to use a large number of rockfall motion statistical data points to train the neural network model. As a result, the model can be used to calculate the horizontal distance of the rockfall motion y of any dangerous rockmass. In the calculation, the rockfall motion sample data can be obtained from historical rockfall data from field investigations, the rockfall numerical simulation, and/or from physical model tests.

2.5.2. Solution for the Influence Area of the Rockfall. The genetic optimization algorithm is a type of mathematical optimization algorithm formed by mimicking the biological evolution process of chromosomes, which undergo reproduction, crossover, and mutation to produce new, fitter chromosomes [30]. Because it is an effective method for solving the optimality problems, the optimality problem shown in (3) can be solved using the genetic optimization algorithm using the following steps:

(1) Randomly generate the initial population P_0 and then use the model expressed in (4)–(8) to calculate the rockfall horizontal distance of each individual mass. Perform the nondominated sorting of the population and give each individual a rank.

(2) Perform the binary tournament selection, crossover, and mutation of P_0 to obtain a new population Q_0 and let $t = 0$.

(3) Combine P_t and Q_t to form a new population R_t and then perform the nondominated sorting of R_t and select the best N individuals to generate a population P_{t+1}.

(4) Reproduce, cross over, and mutate the population P_{t+1} to generate a population Q_{t+1} Qt + 1.

(5) If the number of iterations reaches the preset maximum number, the optimization ends. Otherwise, go to step 1.

Based on the above-mentioned steps, a genetic algorithm (GA) program was written using MATLAB 2012b to calculate the maximum rockfall horizontal distance of any cross profile of the weathered slope mass.

3. Case Study

Multiple episodes of rockfall have occurred historically on the Guanyindong Slope, which is a tourist scenic spot in Zhejiang Province, China. Future rockfall poses a threat to the lives and property of tourists. Taking the Guanyindong Slope as an example, we used the above calculation method to determine the influence area of the Guanyindong Slope, providing a basis for determining and designing disaster prevention and reduction measures for the Guanyindong Slope.

3.1. Overall Characteristics of the Guanyindong Slope. The geographical coordinates of the Guanyindong Slope are 120°36′31.2″ E and 28°42′11.6″ N. The high-steep weathered slope mass has an elevation of approximately 126 m, a slope of 70–88°, and slope aspect towards 310°. There is a $19 \times 17 \times 10\ m^3$ rock cave (the Guanyin cavity) at the bottom of the slope (Figure 3(a)). Inside this rock cave there is a Guanyin statue, which integrates the natural and cultural landscapes and merges the religious and cultural characteristics of the region, making it one of the most important tourist attractions. In the middle of the Guanyindong Slope, there is a weak layer (with an elevation of 230–245 m) that contains a number of cavities formed by weathering (W1–W4 in Figure 3(b)).

The lithology of the slope is composed of Upper Jurassic Jiuliping Formation altered tuff (J3j1) (Figure 4). To further illustrate the microscopic characteristics of the rock, one of the microscopic images of rock samples is shown in Figure 4(b). In addition, due to weathering and flowing water, part of the surface the rock block is grayish black; however, the fresh surface of the rock is grayish white. The bedrock on the surface of the slope is exposed with less vegetation cover (Figure 3(a)). In general, the rockmass is severely weathered with well-developed structural planes (Figure 3(b)). The main controlling structural planes include regional crack structural plane F3 in the steep slope at the Guanyindong entrance (orientation of N40E/80 NW) and the oblique normal fault bedding F8 at the cavity's entrance (orientation of N58W/60 SW). In addition, the slope has gently inclined bedding with the orientation of N85W/10 NE, and a weak intercalated layer has formed between the planes, with steeply inclined cracks with orientation *s* of N32E/88 NW and N33E/72 NW. We also observed that these structural planes cut each other within the rockmass to form large, outwardly inclined blocks, such as block GYD1 (62 m long × 8 m wide × 2 m thick) (Figures 3(c) and 3(d)).

When exposed to external factors such as heavy rainfall, the cracks continue to expand and gradually expand the plastic failure zone of the rockmass and ultimately decrease its strength. Eventually, this will trigger failure phenomena. For example, spalling and rockfall of the rockmass surface as well as local instability and overturning of the block may occur. Based on our field investigations (Figure 5), there have been multiple episodes of rockfall and rolling in this location, with fragments as large as 2 m × 1.5 m × 1 m and as small as 0.05 m × 0.1 m × 0.1 m.

Under the continuous weathering, the rockfall and falling blocks from the surface of the weathered rock slope are uncertain. Thus, it is difficult to predict the position and size of the rockfall block and to track its movement accurately.

3.2. Rockfall Mathematical Model of the Weathered Slope. The rockfall mathematical model of the Guanyindong Slope can be expressed in (3). Based on the field investigations, a local coordinate system was established for the Guanyindong Slope mass (Figures 6(a) and 6(b)).

3.3. Constraints

3.3.1. Position and Numerical Analysis of Dangerous Rockmass that May Be Rockfall. Based on the description in Section 2.2, to determine the position of the dangerous rockmass where rockfall may occur on the Guanyindong Slope, i.e., to determine the ranges of the *x* and *z* values, we used both FLAC^{3D} numerical simulation analysis and geological field investigations.

(1) Establishment of the FLAC^{3D} Numerical Model. The Mohr–Coulomb constitutive model was used in the calculation model. The 3D numerical model was 445 m × 467 m × 258 m, and the model mesh contained 126,438 elements and 31,799 nodes. The upper boundary of the model is the surface, which is set as the free boundary, and the lower boundary is located approximately 45 m below the bottom of the Guanyindong Slope. The model is fixed in the *z* direction and around the boundary in the one-way horizontal axial direction (Figure 7(a)).

(2) Selection of Calculation Parameters. To obtain the calculation parameters, four groups of rock samples (ϕ 50 mm × 100 mm in size, 5 samples in each group) were collected by drilling into the Guanyindong Slope. According to the Standard for Test Methods of Engineering Rockmass (GB/T 50266-2013) (Ministry of Housing and Urban Rural Development of People's Republic of China 2013), a triaxial rock testing machine (TAW2000) was used to conduct the laboratory tests.

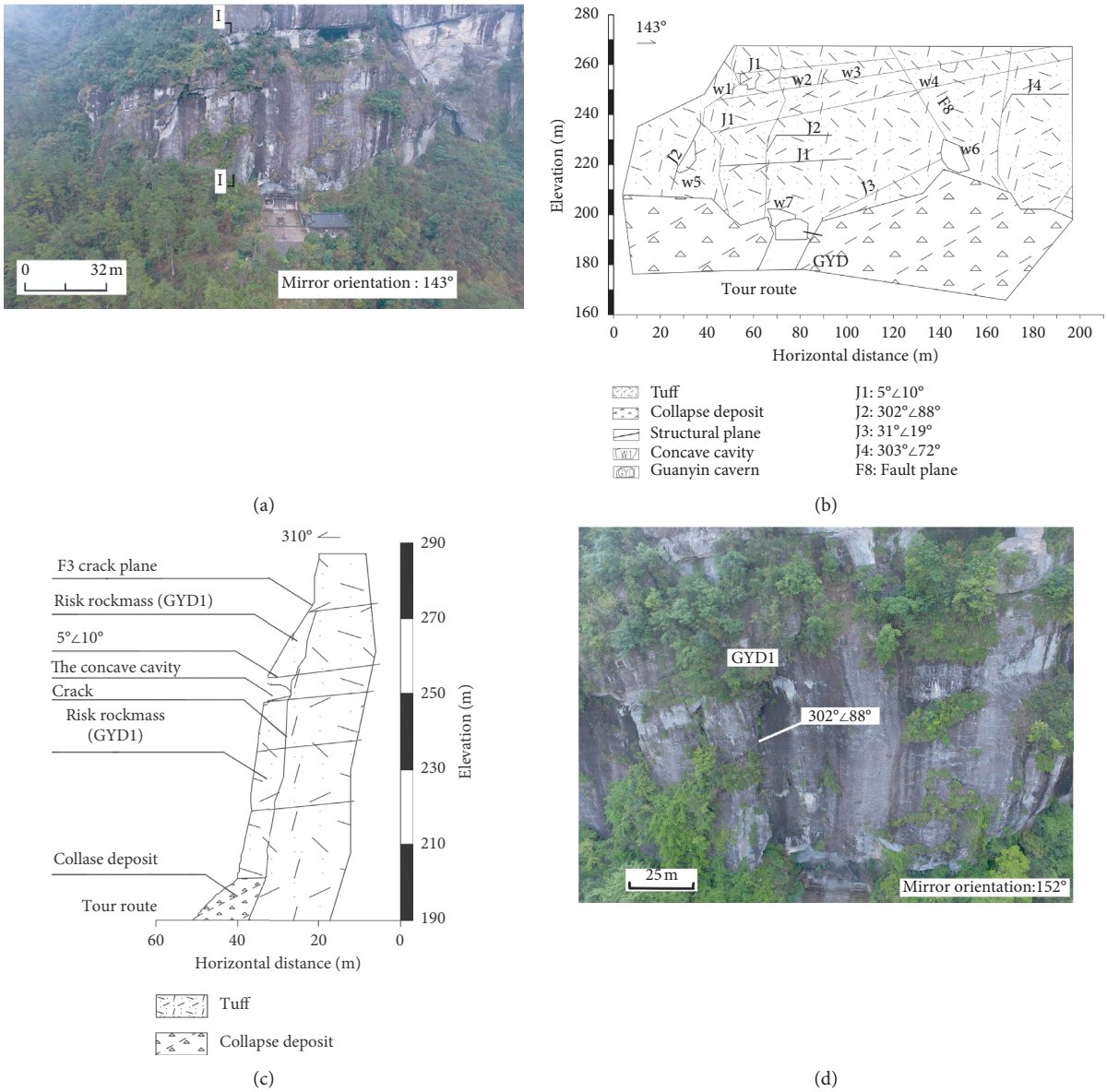

Figure 3: The overall characteristics of the Guanyindong Slope. (a) The overall characteristics of the Guanyindong Slope; (b) the main planar structural distribution of the Guanyindong Slope; and (c) profile I-I.

Figure 4: Rock type and its microscopic characteristics of the Guanyindong Slope. (a) The altered tuff samples; (b) microscopic images of the altered tuff.

Figure 5: Historical rockfall survey results for the Guanyindong Slope.

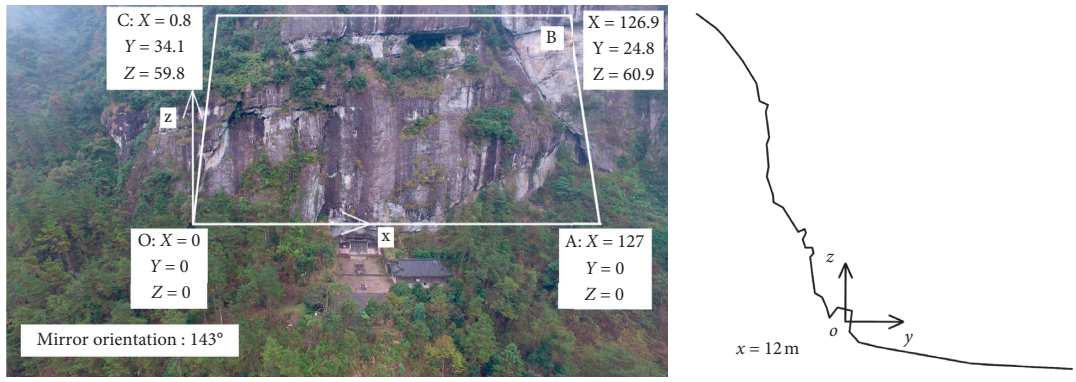

(a) (b)

Figure 6: The local coordinate system for the Guanyindong Slope. (a) The local coordinate system; (b) the local coordinate system of the cross section $x = 12$ m.

Based on the field investigation (Figure 7(d)), we used the orthogonal test method [31] to determine the distribution of the plastic failure of the rockmass using the theory of displacement back analysis [32] (Figure 7(c)). Then, the calculated parameters were used as the physical and mechanical parameters of the Guanyindong rockmass, as shown in Table 1.

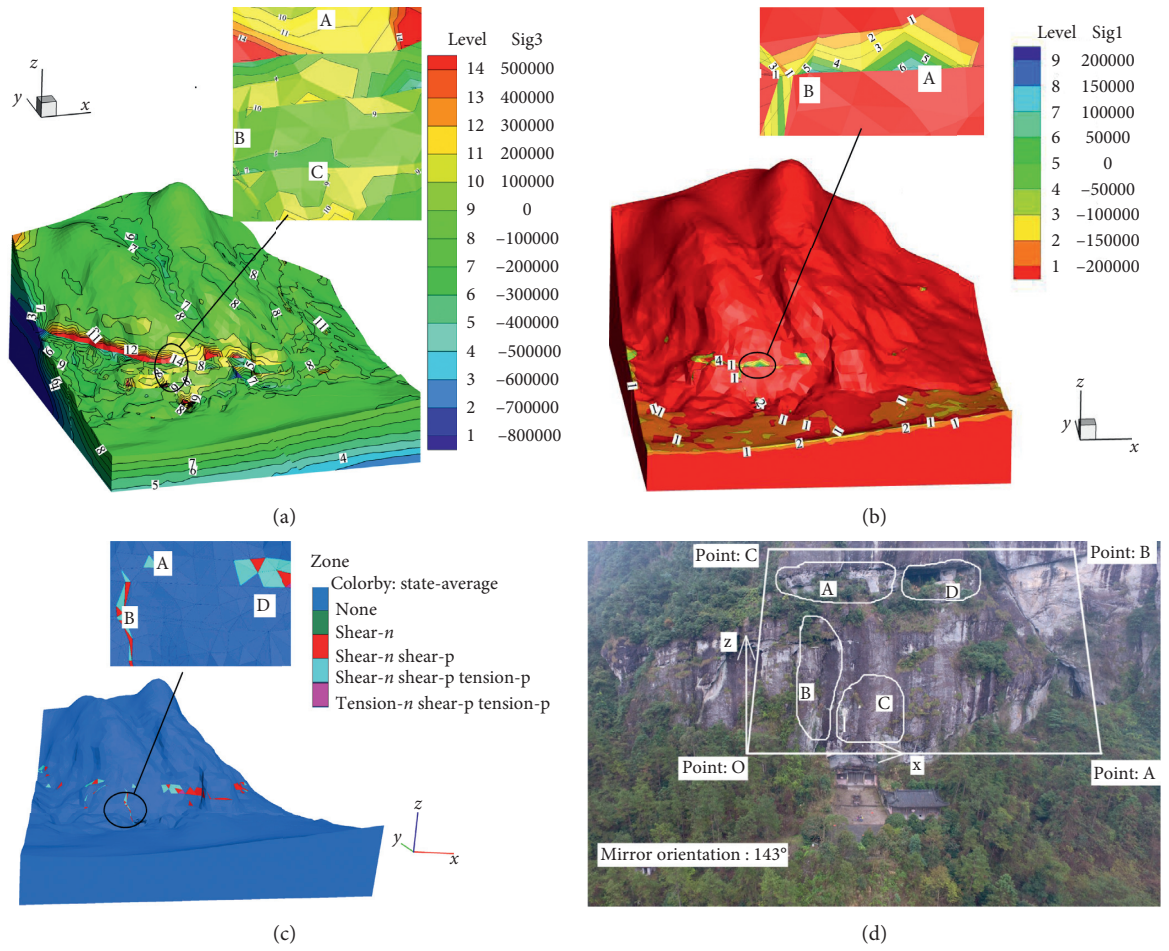

Figure 7: Identification of potential rockfall areas. (a) The minimum principal stress; (b) the maximum principal stress; (c) the plastic failure area; and (d) field investigation results for the failure area.

Table 1: The physical and mechanical parameters of rock samples from Guanyindong Slope.

Rock	Density $\rho((kg)/m)$	Tensile strength $\sigma_t(Pa)$	Cohesion $c(Pa)$	Modulus of elasticity $E(Pa)$	Poisson's ratio	Angle of friction $\varphi(°)$
Tuff (rockmass)	2875	8.25×10^6	2.05×10^7	7.70×10^9	0.18	46.51

(3) Results of the Numerical Simulation Analysis. By numerical simulation, we obtained the results as follows (Figure 7). First, the tensile stress concentration region is mainly distributed in the filling body of the weak intercalated layer between the rockmass above the Guanyindong Slope and the gently inclined bedding (5°∠10°). Second, the plastic failure zone is mainly concentrated in the vicinity of the filling body of the weak intercalated layer and in the cracks (orientation of 302°∠88°) in the gently inclined bedding.

3.3.2. Field Investigation Results. The field investigations provided the following information. Because of continuous weathering, the filling body of the weak intercalated layer was between the gently inclined bedding (orientation of N85W/10 NE) of the Guanyindong Slope experienced rockfall and spalling in multiple locations (see spalling trace locations A and D in Figure 7(d)), forming multiple cavities. The steeply inclined cracks (orientation of N32E/88 NW) and bedding (orientation of N85W/10 NE) cut the rockmass, forming a number of dangerous rockmasses, leading to multiple historical episodes of rockfall and spalling (see spalling trace locations B in Figure 7(d)). Multiple historical events of rockfall and spalling also occurred in the upper part of the Guanyindong Slope (see spalling trace locations C in Figure 7(d)). Authors observed that because areas where the spalling of steep rocks occurred often exhibit fresh grayish-white surfaces, their traces tend to be obvious and are easy to be identified (Figure 7(d)).

3.3.3. Delineation of Potential Rockfall Areas. The rockmass failure distribution obtained from the aforementioned field investigations (Figure 7(d)) is in a good agreement with the plastic failure zone and tensile stress distribution zone (Figures 7(a)–7(c)) determined from the numerical simulation. According to Section 2.2.1, we can delineate the potential rockfall area of the Guanyindong Slope mass, as shown in Figure 7(d). The value range is

$$\{(x,z) \mid x \in (0,127), \quad z \in (0,60)\}. \tag{9}$$

3.4. Estimation of the Mass of the Potentially Rockfall Dangerous Rockmass. According to Section 2.2.2, the field investigations and a combination of UAV and 3D laser scanning were carried out. The results revealed that the volume of historical rockfall blocks from the Guanyindong Slope was from $0.0005\,\mathrm{m}^3$ to $3\,\mathrm{m}^3$. Based on the Guanyindong Slope's rock density of $2875\,\mathrm{kg/m}^3$ (Table 1), we estimate the value range of the mass m of the potentially rockfall rockmass to be

$$m \in [1.4, 9487]. \tag{10}$$

3.5. Calculation of the Influence Area of the Rockfall

3.5.1. Calculation Model. According to the above analysis, the mathematical model for determining the rockfall area of the Guanyindong Slope is

$$\begin{aligned} \max \quad & y = \max f_x(z, m_v), \\ \text{s.t} \quad & \begin{cases} x \in [0,127], \\ z \in [0,60], \\ m_v \in [1.4, 9487]. \end{cases} \end{aligned} \tag{11}$$

The procedure for solving the calculation model is as follows:

(1) Ten cross sections within the value range of x, i.e., $x = (12, 24, 36, 48, 60, 72, 84, 96, 108, 120)$, were defined.

(2) The objective function $y = f_x(z, m_v)$ in (11)fd11 is an uncertainty function, which was represented using the neural network model described in Section 2.3.1.

(3) Using the historical rockfall data, the normal and tangential coefficients of restitution [33–35] and the friction angle of the Guanyindong Slope were determined using the theory of displacement back analysis (Figure 8) [32]. Based on the parameters, RocFall^{2D} software was used to simulate possible rockfall events for each cross profile and to obtain sample data for these rockfall events. In order to reduce the error of slope geometry to numerical simulation, according to the principle of aerial photogrammetry [36], the slope image data are acquired by using the tilt photography of five routes including East, South, West, North, and orthoimage with the help of PHANTOM 4 RTK Unmanned Aerial Vehicle (UAV). Among them, the UAV camera of the East, South, West, and North routes forms a 45°angle with the horizontal plane, and the UAV camera of the orthoimage route forms a 90°angle with the horizontal plane. Using context Capture Center Master and other software applications, combined with the principle of reverse modeling [37], the collected image data is generated into a three-dimensional model and 3D point cloud, and then the position, shape, size, and other data of the slope section are identified (Figures 1 and 8). The computer program for the neural network model, which was constructed in training step (2), was written using MATLAB. Then, the trained neural network was used to predict possible rockfall events.

Using the GA described in Section 2.3.2, a relevant program was prepared using MATLAB 2012b. Then, the calculation model represented by (11) was solved to obtain the maximum possible rockfall horizontal distance of each cross profile.

3.5.2. Calculation Model Solution. According to the model solving procedure described in Sections 3.5.1 and 2.3.1, the RocFall™ was used to obtain neural network training data for each cross section of the Guanyindong Slope. Because the historical rockfall data for the Guanyindong Slope obtained from the field investigations was not sufficient to satisfy the requirements of the neural network training, we obtained the normal and tangential restitution coefficients and the friction angle of the rockmass based on the theory of displacement back analysis [32] using historical rockfall data (see Figure 8). Then, numerical simulations of the possible rockfall events of each cross profile of the slope were carried out to obtain the necessary corresponding sample training data.

(1) Determination of the Simulation Parameters of the Rockfall Motion. The historical rockfall events were back-calculated as shown in Figures 8(a) and 7(b). The size of the rockfall rock was $1.8\,\mathrm{m} \times 1.5\,\mathrm{m} \times 0.75\,\mathrm{m}$, and the obtained parameters for the rockfall of the rockmass included a normal restitution coefficient of 0.53, a tangential restitution coefficient of 0.75, and a friction angle of 46.5°.

The rockfall motion was verified using back-calculated the historical rockfall events shown in Figures 8(c) and 7(d). The size of the rockfall rock was $2\,\mathrm{m} \times 1.5\,\mathrm{m} \times 1\,\mathrm{m}$. The simulation results by rockfall are consistent with the field investigations and confirm the validity of the above parameters.

(2) Acquisition of Sample Data. According to the rockfall parameters obtained from the above, we used the uniform design table to design a rockfall simulation test for each cross profile and to obtain training sample data for the neural network of each cross profile. Table 2 shows the orthogonal factor level table of the cross profile $x = 12\,\mathrm{m}$ designed using the uniform design table $U_{30}^{*}(30^{12})$. Table 3 presents the

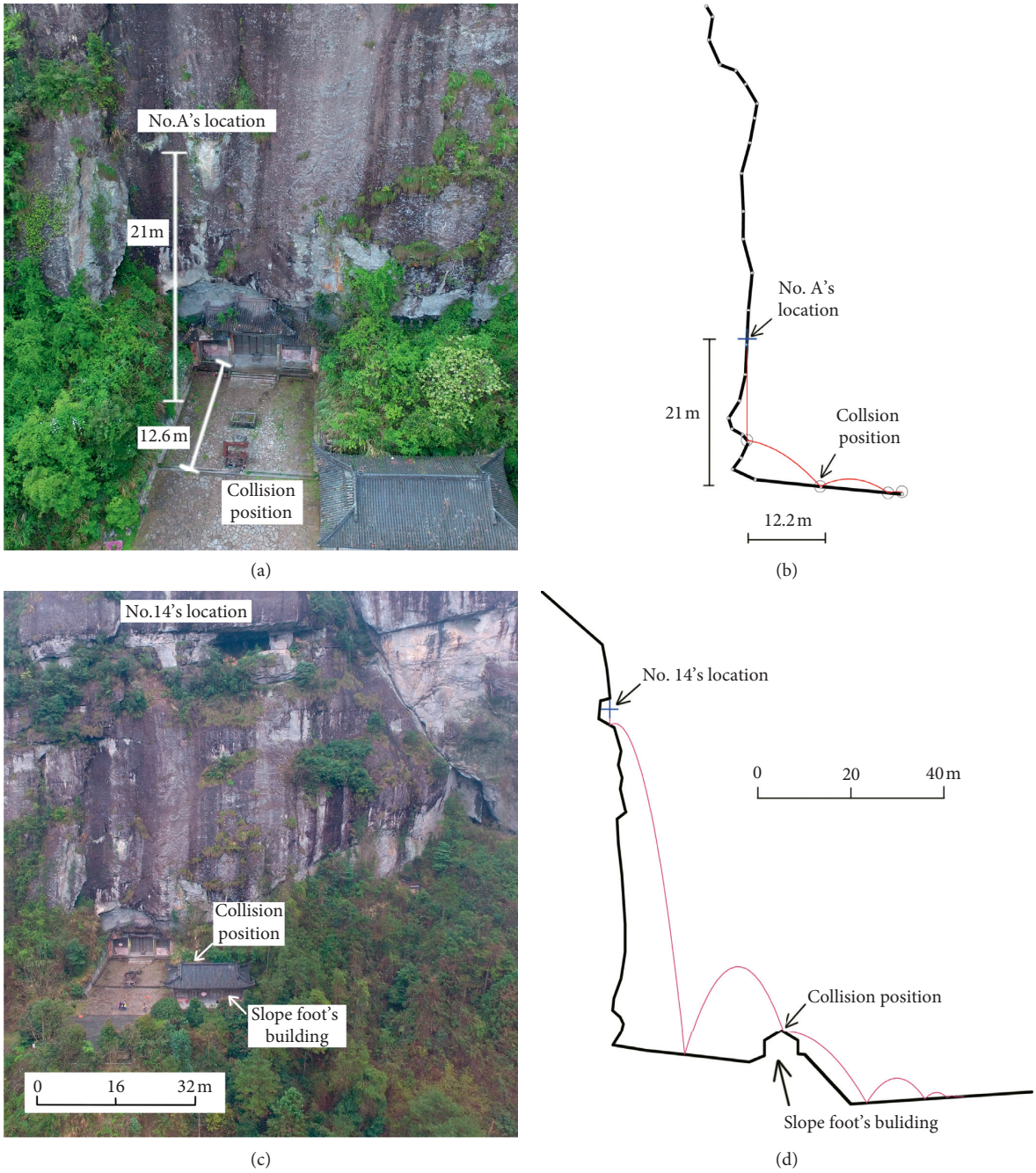

Figure 8: The back analysis mechanical parameters of the rockfall motion. (a) Historical rockfall event 1; (b) back analysis results for historical rockfall event 1; (c) historical rockfall event 2; and (d) back analysis results for historical rockfall event 2.

experimental arrangement and results of the numerical simulation test, i.e., the training sample data of cross profile $x = 12$ m (the coordinate system is shown in Figure 6(b)). Due to space limitations, only data for cross profile $x = 12$ m is reported.

The experimental arrangement and results are shown in Table 3.

(3) Calculation of the Influence Area of the Rockfall of Each Cross Section. The GA calculation program was created using MATLAB 2012b according to the method described in Section 2.3.2. Then, it was used to solve the maximum influence area of each profile and the height Z and mass M of the corresponding rockfall rockmass. The calculation results are shown in Table 4.

4. Discussion of the Calculation Results

For comparison, we used Rocscience RocFall 6.0 to conduct a numerical simulation of the calculation results again. The results indicate that the deviation between the results of the rockfall numerical simulation and those of the GA

Table 2: The orthogonal factor levels of cross section.

Level	Factor	
	Z	M
1	6	1.40
2	7.86	328.49
3	9.72	655.58
4	11.59	982.67
5	13.45	1309.76
6	15.31	1636.85
7	17.17	1963.94
8	19.03	2291.03
9	20.90	2618.12
10	22.76	2945.21
11	24.62	3272.30
12	26.48	3599.39
13	28.34	3926.48
14	30.21	4253.57
15	32.07	4580.66
16	33.93	4907.74
17	35.79	5234.83
18	37.66	5561.92
19	39.52	5889.01
20	41.38	6216.10
21	43.24	6543.19
22	45.10	6870.28
23	46.97	7197.37
24	48.83	7524.46
25	50.69	7851.55
26	52.55	8178.64
27	54.41	8505.73
28	56.28	8832.82
29	58.14	9159.91
30	60	9487.00

Z is the elevation of rockfall rock. M is mass of rockfall rock.

Table 3: The experimental arrangements and results.

Experiment	Factor		Experimental result y
	Z	M	
1	6	6870.28	−8.111
2	7.86	3926.48	−8.161
3	9.72	982.67	−8.030
4	11.59	8178.64	−10.884
5	13.45	5234.83	−15.378
6	15.31	2291.03	−6.621
7	17.17	9487.00	−6.211
8	19.03	6543.19	−5.252
9	20.90	3599.39	75.662
10	22.76	655.58	78.820
11	24.62	7851.55	87.112
12	26.48	4907.74	89.953
13	28.34	1963.94	86.387
14	30.21	9159.91	89.403
15	32.07	6216.10	91.772
16	33.93	8832.82	99.755
17	35.79	6870.28	102.602
18	37.66	7524.46	104.472
19	39.52	4580.66	−20.093
20	41.38	1636.85	96.014
21	43.24	8832.82	96.387
22	45.10	5889.01	−18.076
23	46.97	2945.21	−24.929
24	48.83	1.40	−25.123
25	50.69	7197.37	−26.288
26	52.55	4253.57	−27.473
27	54.41	1309.76	−28.655
28	56.28	8505.73	−29.959
29	58.14	5561.92	−30.994
30	60	2618.12	−33.952

Z is the elevation of rockfall rock. M is mass of rockfall rock.

calculations is only 0.096–2.491 m (Figure 9). In particular, the smallest and largest deviations occur for cross profiles $x = 72$ m and $x = 120$ m, respectively (Figure 9). Therefore, the calculation results are believed to be reliable.

4.1. Application of the Calculation Results. According to the above calculation and analysis, we obtained a safe horizontal distance for the engineering application of the Guanyindong Slope. This is shown as follows:

$$y = \max f_x(z, m_v). \tag{12}$$

Next, the maximum horizontal distance values of the potential rockfall of the different cross profiles were connected to form a spline curve in order to obtain the rockfall influence area on the Guanyindong Slope (Figure 10). The recorded historical rockfall events (labeled as historical rockfalls A to M in Figures 5 and 10) were identified in the field investigations and the positions of the rockfall of the dangerous rockmasses all fall within the calculated influence area of the rockfall. It should be noted that the department in charge of this scenic spot now closes the Guanyindong scenic spot due to the potential rockfalls that would threaten the safety of tourists. Then, the optimized design was carried out based on the above research results.

4.2. Countermeasures. According to Figure 10, to ensure the safety of tourists in the Guanyindong scenic spot, the following disaster prevention and mitigation measures should be considered; see Figure 11(a).

(1) Abandon the original 151 m long trail into the Guanyindong scenic spot and replace it with shrubs and other vegetations to keep people out of the influence area of potential rockfall. Then, construct a new tourist route (the improved tourist route (South) or the improved tourist route (North)) (as shown in Figure 10).

(2) The improved tourist route (North) leads to the cobblestone path at Wanxian Bridge. First, it extends to the northeast, and then it turns and extends to the southeast, which avoids the potential rockfall influence area. In addition, a tunnel can be constructed in this location at an elevation of approximately 200 m to provide access to the northern end of the Guanyindong scenic area. The improved tourist

Table 4: The calculation results for the influence range of each cross section of the Guanyindong Slope.

Slope section position x (m)	Elevation of rockfall rock Z (m)	Mass of rockfall rock M (kg)	Position of rockfall rock y (m)
12	38.705	4986.204	111.616
24	60	4196.453	102.397
36	41.841	7240.130	51.735
48	37.205	2151.947	70.18
60	60	7601.522	88.684
72	60	4351.76	90.131
84	51.640	2836.387	76.176
96	60	3658.595	90.930
108	60	3527.153	87.308
120	59.456	4974.903	117.478

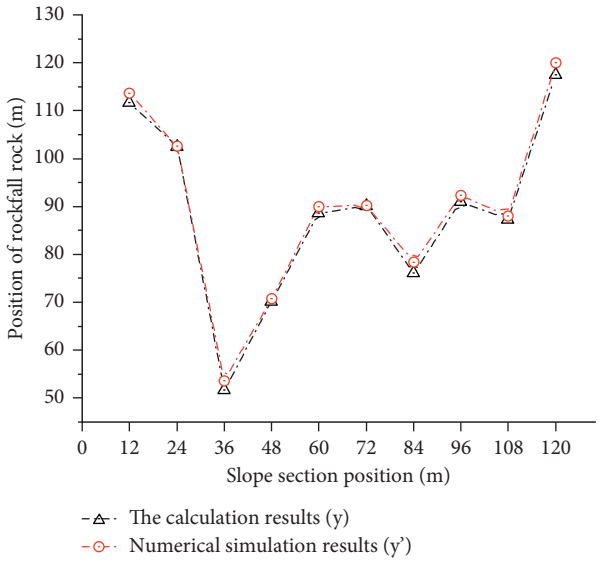

Figure 9: The comparison between the calculation results and the numerical simulation results.

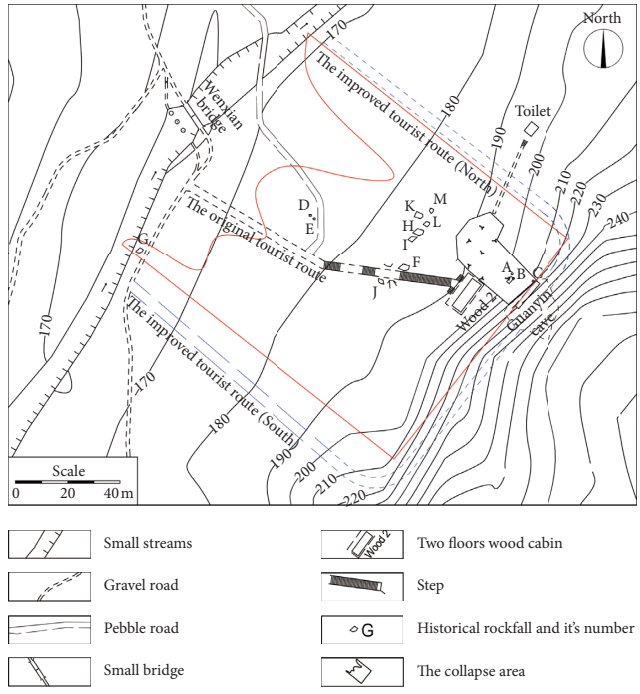

Figure 10: The rockfall influence area of the Guanyindong Slope.

route (North) is 202 m long, including a 41.8 m long and 2 m wide tunnel. This scheme is 51 m longer than the original tourist route. In addition, we recommend that a concrete canopy be added to protect tourists from rockfalls caused by the steep weathered slope at the entrance.

(3) The improved tourist route (South) follows the original cobblestone path (the southward extension of Wanxian Bridge) but then follows a new route on the southwestern side of the influence area of the rockfall. A tunnel can be constructed in this location at an elevation of approximately 200 m to access the southern side of the Guanyindong scenic area. This route is 203 m long, including the 107 m long and 2 m wide tunnel. This scheme is 52 m longer than the original tourist route. A concrete canopy should also be installed at the tunnel's entrance to ensure the safety of tourists.

(4) The original terrace in front of the Guanyindong scenic spot is within the influence area of the rockfall. Historical records include multiple rock rockfall and rockfall events occurring in this area. For the safety of the tourists, this terrace should be abandoned and converted into landscaped vegetation. Visitors should be prohibited from entering this area.

(5) For areas with severe weathering such as weak regolith at an elevation of about 250 m, a new method for surface vegetalization of slope reinforced with anchoring bar and shotcrete structure [38] can be adopted for reinforcement. The prestressed bolt was implanted into the risk rockmass (GYD1). The initial elevation of the bolt layout is 210 m, and a total of 7 layers were arranged with each layer having a height of 5 m. The horizontal spacing of the bolt arrangement was 5 m. The dip angle was 30°, and the prestress was 400 KN. The length of bolt was 15 m, the length of free section was 5 m, and the length of anchorage section was 8 m. The bolt was made of 4 × 7 (ϕ5 mm) steel strand (Figure 11(a)). Numerical

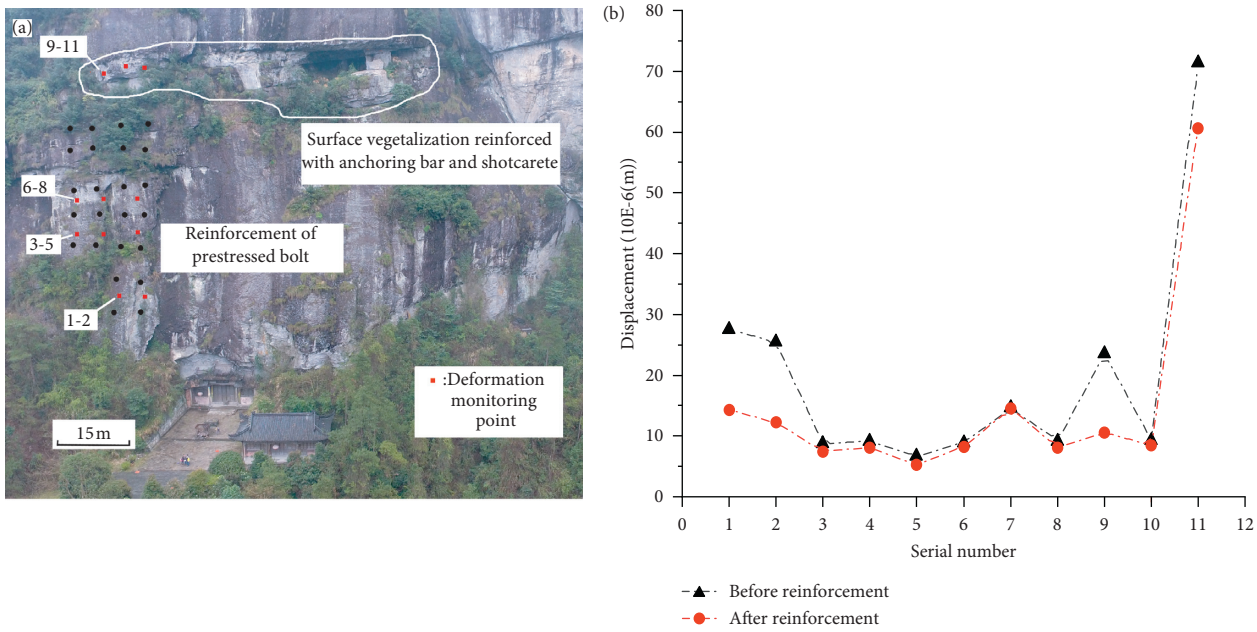

Figure 11: Engineering reinforcement measures. (a) Engineering reinforcement plan; (b) deformation monitoring results.

simulation results show that the displacements of monitoring point were improved obviously after reinforcement (Figure 11(b)).

5. Conclusions

Since predicting the rockfall trajectory and calculating the influence area of rockfall are of profound importance in studying the uncertainty of rockfall and the active protection against rockfall hazards, a reliable estimate of the influence area of rockfall is crucial to the design of passive preventative methods for preventing rockfall. We studied the calculation method of the influence area of rockfall, by taking an engineering case in a tourist scenic spot in Zhejiang Province, China.

(1) The results of field investigations and numerical simulation indicate that the area of tensile stress concentration and plastic failure is the potential rockfall area where the rockmass will fall from the surface of weathered rock slope.

(2) The normal and tangential restitution coefficients and the friction angle of the weathered rock slope for the rockfall numerical simulation were obtained based on back analysis of historical rockfall events. The numerical simulation results based on these parameters can be used as learning samples for the BP neural network. Then, the motion and influence area of the potential rockfall can be effectively predicted. However, the RocFall^{2D} numerical simulation results still deviated slightly from the historical data.

(3) The prediction of the influence area based on optimization theory, neural network technology, and the genetic optimization algorithm provides a new way to eliminate rockfall uncertainties and can be used as a guidance in the prevention of rockfall hazards.

Data Availability

The authors do not have permission to share data.

Conflicts of Interest

The authors declare that there are no conflicts of interest regarding the publication of this paper.

Acknowledgments

This research was funded by the Zhejiang Province Welfare Technology Applied Research Project, Grant no. 2017C33190, the Strategic Priority Research Program of the Chinese Acadamy of Sciences, Grant no. XDA23090402 and the National Natural Science Foundation of China, Grant no. 41672321.

Supplementary Materials

GA Program. (*Supplementary Materials*)

References

[1] L. K. A. Dorren, "A review of rockfall mechanics and modelling approaches," *Progress in Physical Geography: Earth and Environment*, vol. 27, no. 1, pp. 69–87, 2003.

[2] N. Zhang, J. S. Shen, C. Lin, A. Arulrajah, and J.-C. Chai, "Investigation of a large ground collapse and countermeasures during mountain tunnelling in Hangzhou: a case study," *Bulletin of Engineering Geology and the Environment*, vol. 78, no. 2, pp. 991–1003, 2019.

[3] T. Topal, M. Akin, and U. A. Ozden, "Assessment of rockfall hazard around Afyon Castle, Turkey," *Environmental Geology*, vol. 53, no. 1, pp. 191–200, 2007.

[4] C. Michoud, M.-H. Derron, P. Horton et al., "Rockfall hazard and risk assessments along roads at a regional scale: example

in Swiss Alps," *Natural Hazards and Earth System Sciences*, vol. 12, no. 3, pp. 615–629, 2012.

[5] S. G. Evans and O. Hungr, "The assessment of rockfall hazard at the base of talus slopes," *Canadian Geotechnical Journal*, vol. 30, no. 4, pp. 620–636, 1993.

[6] Z. Yao, H. Zaiqiang, and X. Zhijia, "A new method of assessing the collapse sensitivity of loess," *Bulletin of Engineering Geology and the Environment*, vol. 77, no. 4, pp. 1287–1298, 2018.

[7] L. K. A. Dorren, F. Berger, C. Le Hir, E. Mermin, and P. Tardif, "Mechanisms, effects and management implications of rockfall in forests," *Forest Ecology and Management*, vol. 215, no. 1–3, pp. 183–195, 2005.

[8] A. M. Ritchie, *Evaluation of Rockfall and Its Control*, Highway Research Record, Washington, DC, USA, 1963.

[9] A. Volkwein, K. Schellenberg, V. Labiouse et al., "Rockfall characterisation and structural protection—a review," *Natural Hazards and Earth System Sciences*, vol. 11, no. 9, pp. 2617–2651, 2011.

[10] A. Azzoni and M. H. d. Freitas, "Experimentally gained parameters, decisive for rock fall analysis," *Rock Mechanics and Rock Engineering*, vol. 28, no. 2, pp. 111–124, 1995.

[11] L. K. A. Dorren, F. Berger, and U. S. Putters, "Real-size experiments and 3-D simulation of rockfall on forested and non-forested slopes," *Natural Hazards and Earth System Science*, vol. 6, no. 1, pp. 145–153, 2006.

[12] D. Trappmann, M. Stoffel, and C. Corona, "Achieving a more realistic assessment of rockfall hazards by coupling three-dimensional process models and field-based tree-ring data," *Earth Surface Processes and Landforms*, vol. 39, no. 14, pp. 1866–1875, 2014.

[13] D. Bozzolo and R. Pamini, "Simulation of rock falls down a valley side," *Acta Mechanica*, vol. 63, no. 1–4, pp. 113–130, 1986.

[14] T. J. Pfeiffer and T. D. Bowen, "Computer simulation of rockfalls," *Environmental & Engineering Geoscience*, vol. xxvi, no. 1, pp. 135–146, 1989.

[15] F. Agliardi and G. B. Crosta, "High resolution three-dimensional numerical modelling of rockfalls," *International Journal of Rock Mechanics and Mining Sciences*, vol. 40, no. 4, pp. 455–471, 2003.

[16] G. B. Crosta and F. Agliardi, "Parametric evaluation of 3D dispersion of rockfall trajectories," *Natural Hazards and Earth System Science*, vol. 4, no. 4, pp. 583–598, 2004.

[17] S. Perret, F. Dolf, and H. Kienholz, "Rockfalls into forests: analysis and simulation of rockfall trajectories? considerations with respect to mountainous forests in Switzerland," *Landslides*, vol. 1, no. 2, pp. 123–130, 2004.

[18] M. Jaboyedoff, J. P. Dudt, and V. Labiouse, "An attempt to refine rockfall hazard zoning based on the kinetic energy, frequency and fragmentation degree," *Natural Hazards and Earth System Science*, vol. 5, no. 5, pp. 621–632, 2005.

[19] K. Messenzehl, H. Meyer, J.-C. Otto, T. Hoffmann, and R. Dikau, "Regional-scale controls on the spatial activity of rockfalls (Turtmann Valley, Swiss Alps)—a multivariate modeling approach," *Geomorphology*, vol. 287, pp. 29–45, 2017.

[20] L. K. A. Dorren and A. C. Seijmonsbergen, "Comparison of three GIS-based models for predicting rockfall runout zones at a regional scale," *Geomorphology*, vol. 56, no. 1-2, pp. 49–64, 2003.

[21] H. Lan, C. Derek Martin, and C. H. Lim, "RockFall analyst: a GIS extension for three-dimensional and spatially distributed rockfall hazard modeling," *Computers & Geosciences*, vol. 33, no. 2, pp. 262–279, 2007.

[22] T. Heckmann, L. Hilger, L. Vehling, and M. Becht, "Integrating field measurements, a geomorphological map and stochastic modelling to estimate the spatially distributed rockfall sediment budget of the upper Kaunertal, Austrian central Alps," *Geomorphology*, vol. 260, pp. 16–31, 2016.

[23] P. Frattini, G. B. Crosta, and F. Agliardi, "Rockfall characterization and modeling," in *Landslides*, Cambridge University Press, Cambridge, UK, 2012.

[24] X. Wang, P. Frattini, G. B. Crosta et al., "Uncertainty assessment in quantitative rockfall risk assessment," *Landslides*, vol. 11, no. 4, pp. 711–722, 2014.

[25] W. Peng, *FLAC3D Practical Tutorials*, Machinery Industry Press, Beijing, China, 2008, in Chinese.

[26] Ministry of Housing and Urban Rural Development of People's Republic of China, *Standard for Test Method of Engineering Rock Mass*, China Planning Publishing House, Beijing, China, 2013, in Chinese.

[27] X. H. Liao, X. Huang, J. L. Shi, and Y. L. Sun, "Forecast model about compressive strength of recycle aggregate concrete base on BP neutral network," *Journal of Nanjing Forestry University*, vol. 34, pp. 105–108, 2010, in Chinese.

[28] Z. Qiao, "Study on decision support method based on extenics and BP neural network," in *Proceedings of the Seventh International Conference on Fuzzy Systems and Knowledge Discovery*, August 2010.

[29] L. Han, *Artificial Neural Network Theory, Design and Application*, Chemical Industry Press, Beijing, China, 2007, in Chinese.

[30] G. Xuan and R. Cheng, *Genetic Algorithm and Engineering Optimization*, Tsinghua University Press, Beijing, 2004, in Chinese.

[31] W. Liu, *Applied Statistics Textbook Series, Experimental Design*, Tsinghua University Press, Beijing, China, 2005, in Chinese.

[32] Y. Sun and L. Zhang, "Study on displacement back analysis of spatial variability of soil slope," in *Proceedings of the Geo-Shanghai International Conference*, May 2018.

[33] L.-p. Li, S.-q. Sun, S.-c. Li, Q.-q. Zhang, C. Hu, and S.-s. Shi, "Coefficient of restitution and kinetic energy loss of rockfall impacts," *KSCE Journal of Civil Engineering*, vol. 20, no. 6, pp. 2297–2307, 2016.

[34] V. Labiouse and B. Heidenreich, "Half-scale experimental study of rockfall impacts on sandy slopes," *Natural Hazards and Earth System Science*, vol. 9, no. 6, pp. 1981–1993, 2009.

[35] O. Buzzi, A. Giacomini, and M. Spadari, "Laboratory investigation on high values of restitution coefficients," *Rock Mechanics and Rock Engineering*, vol. 45, no. 1, pp. 35–43, 2012.

[36] W. Chunxiang, L. Xiao, and S. Qingwei, *Aerial Photogrammetry*, Yellow River Conservancy Press, Zhengzhou, China, 2011, in Chinese.

[37] S. Yan and X. Binfei, *Imageware Technical Basis of Reverse Modeling*, Tsinghua University Press, Beijing, China, 2006, in Chinese.

[38] Z. Luqing, Y. Zhifa, S. Yanjun, and Y. Liu, "New method for surface vegetalization of slopes reinforced with anchoring bar and shotcrete structure," *Chinese Journal of Rock Mechanics and Engineering*, pp. 42–48, 2007, in Chinese.